Cosmogenic ^{3}He and ^{10}Be chronologies of the late Pinedale northern Yellowstone ice cap, Montana, USA

Joseph M. Licciardi*, Peter U. Clark — Department of Geosciences, Oregon State University, Corvallis, Oregon 97331, USA
Edward J. Brook — Department of Geology, Washington State University, Vancouver, Washington 98686, USA
Kenneth L. Pierce — U.S. Geological Survey, Northern Rocky Mountain Science Center, Montana State University, Bozeman, Montana 59717, USA
Mark D. Kurz — Department of Marine Chemistry and Geochemistry, Woods Hole Oceanographic Institution, Woods Hole, Massachusetts 02543, USA
David Elmore, Pankaj Sharma — Department of Physics, PRIME Lab, Purdue University, West Lafayette, Indiana 47907, USA

ABSTRACT

Cosmogenic ^{3}He and ^{10}Be ages measured on surface boulders from the moraine sequence deposited by the northern outlet glacier of the Yellowstone ice cap indicate that the outlet glacier reached its terminal position at 16.5 ± 0.4 ^{3}He ka and 16.2 ± 0.3 ^{10}Be ka, respectively. Concordance of these ages supports the scaled production rates used for ^{3}He (118.6 ± 6.6 atoms · g^{-1} · yr^{-1}) and ^{10}Be (5.1 ± 0.3 atoms · g^{-1} · yr^{-1}) (±2σ at high latitudes at sea level). Two recessional moraines upvalley from the terminal moraine have mean ages of 15.7 ± 0.5 ^{10}Be ka and 14.0 ± 0.4 ^{10}Be ka, respectively, and a late-glacial flood bar was deposited at 13.7 ± 0.5 ^{10}Be ka. These cosmogenic chronologies identify a late Pinedale glacial maximum in northern Yellowstone that is significantly younger than previously thought, and they suggest deglaciation of the Yellowstone plateau by ~14 ^{10}Be ka.

Keywords: cosmogenic elements, geochronology, glacial geology, Pinedale glaciation, Yellowstone.

INTRODUCTION

The late Pleistocene Yellowstone ice cap was the largest independent glacier system in the western United States. In the past 25 years, many innovative geochronological methods have been used to develop a record of fluctuations of this ice cap (Pierce et al., 1976; Pierce, 1979; Sturchio et al., 1994), and these have formed a cornerstone of understanding the timing of the last (Pinedale) glaciation for much of the Rocky Mountains (Porter et al., 1983). None of the ages constraining the history of the Yellowstone ice cap, however, directly constrains the age of moraine-building events when the ice-cap margin was at or near its maximum size. Here, we use the cosmogenic nuclides ^{3}He and ^{10}Be to directly date a well-preserved moraine sequence deposited by the large outlet glacier that drained the northern Yellowstone ice cap (Fig. 1). Our exposure ages, combined with existing chronological data from this region, establish a new record of late Pinedale millennial-scale fluctuations of this outlet glacier. The high coherency and reproducibility of the ^{3}He and ^{10}Be data demonstrate the utility of the surface exposure dating technique for developing high-resolution glacial chronologies.

SAMPLING

The sampled deposits have well-preserved morphology, large surface boulders of granitic lithologies and occasional basalt, and are covered only by grasslands. All boulders selected for sampling appeared pristine and undisturbed, as evidenced by glacial polish, striae, or negligible surface pitting that indicated limited erosion or spalling. Samples were collected from horizontal boulder surfaces on stable parts of the landforms. Only the largest boulders (>1 m above the surface) were sampled, in order to reduce potential problems of soil and snow cover.

We sampled ten granitic and eight basaltic boulders from the outermost set of end moraines (Eightmile terminal moraines) and associated outwash fan that mark the limit of the northern Yellowstone outlet glacier at the last Pinedale glacial maximum (Pierce, 1979) (Fig. 1), providing a rare opportunity to measure cosmogenic ^{10}Be and ^{3}He concentrations on the same landform. We also sampled eight granitic boulders from the recessional Chico moraines that are 7 km upvalley (Fig. 1B) and ten granitic boulders from the recessional Deckard Flats moraines that were deposited another 47 km upvalley (Pierce, 1979) (Fig. 1C). Finally, we sampled seven granitic boulders from a late-glacial flood deposit in the Yellowstone River valley within the limit of the Deckard Flats event (Fig. 1C); this deposit probably formed during a large glacial outburst flood by release of an ice-dammed lake upvalley from Deckard Flats (Pierce, 1979).

COSMOGENIC ^{3}He AND ^{10}Be MEASUREMENTS

For the ^{3}He measurements, olivine phenocrysts were separated from basalt samples by crushing, sieving, magnetic separation, and handpicking. The cosmogenic ^{3}He content of the olivine was measured by gas mass spectrometry at the Woods Hole Oceanographic Institution following previously described methodology (see Kurz, 1986; Kurz et al., 1990, 1996; and Licciardi et al., 1999, for procedural details, reproducibility, and blanks). We measured ^{10}Be in quartz, using standard techniques of rock crushing and grinding, isolation of quartz by repeated acid leaching (Kohl and Nishiizumi, 1992), and separation of beryllium by ion-exchange chemistry and selective precipitation techniques (see Licciardi, 2000, for full procedural details). All ^{10}Be concentrations were determined by accelerator mass spectrometry (AMS) at the PRIME Lab facility at Purdue University (Sharma et al., 2000). Cosmogenic ^{3}He and ^{10}Be concentrations at each sample site were normalized to the rock surface by accounting for sample thickness and density and by using the estimated dependence of isotope production with depth (Kurz, 1986; Brown et al., 1992). Shielding by surrounding topography is <10° at all sites; thus, no corrections for this phenomenon were necessary.

SCALING METHODS AND PRODUCTION RATES

We use the mean of the cosmogenic ^{3}He production rate calibrations derived from the well-dated Tabernacle Hill flow and Bonneville flood deposits (Cerling and Craig, 1994) for the helium age calculations because these calibration sites are very close in altitude and latitude to the Yellowstone sample locations and are nearly identical in age to the

*Present address: Department of Marine Chemistry and Geochemistry, Woods Hole Oceanographic Institution, Woods Hole, Massachusetts 02543, USA; e-mail: jlicciardi@whoi.edu.

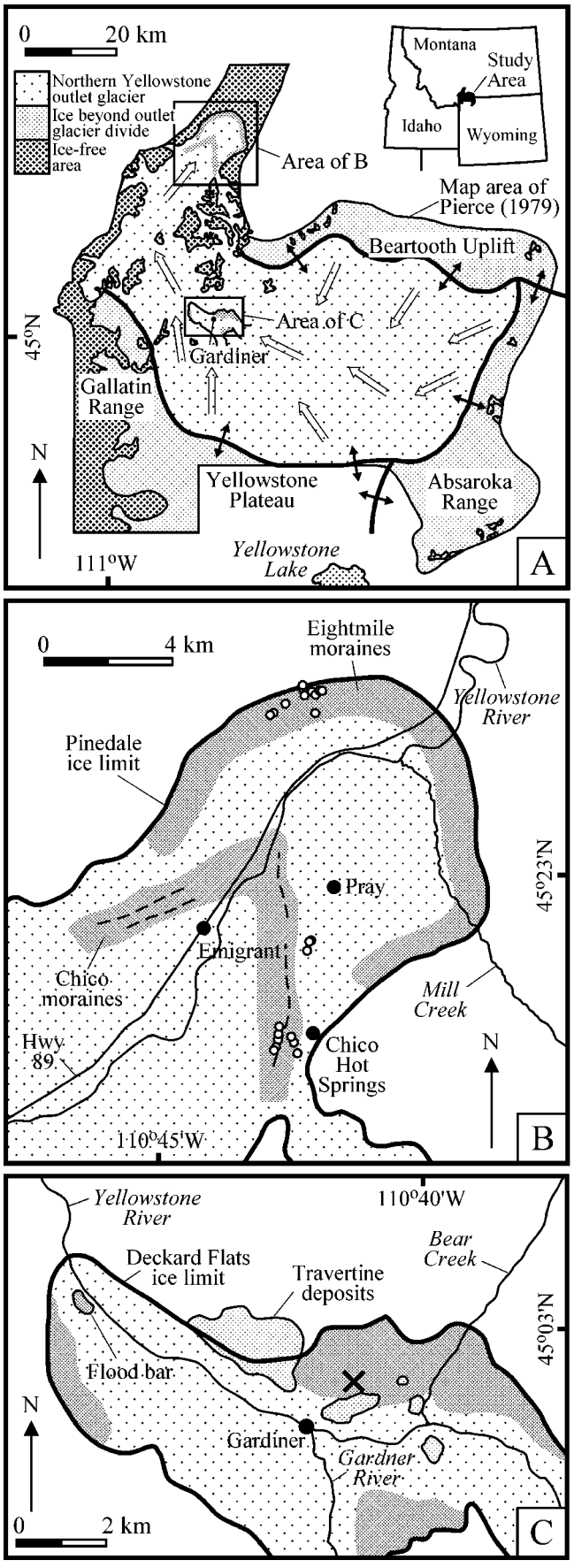

Figure 1. Glacial deposits in northern Yellowstone area. Adapted from Pierce (1979). A: Northern Yellowstone ice cap. Thick black lines with double-pointed arrows indicate main ice divides of various ice masses that fed northern Yellowstone outlet glacier. Open arrows indicate flow directions of major ice drainage ways. B: Sample sites on Eightmile and Chico moraines. Sites are concentrated in areas that contained largest and most suitable boulders. Dashed lines show prominent crests in Chico moraine complex. Three sampled boulders located 2 km south-southwest of town of Pray are considered to belong to proximal part of Eightmile moraines. C: Sample sites on Deckard Flats moraines and late-glacial flood deposit. Individual sample sites on Deckard Flats moraines (dark stipple) are clustered in location marked × and sites on flood bar are clustered within outline of deposit. Travertine deposits are those used by Sturchio et al. (1994) to construct their U-series chronology (see text).

exposure durations calculated here. These two calibration sites yield a weighted mean production rate of 118.6 ± 6.6 atoms · g^{-1} · yr^{-1} (±2σ; in olivine, at high latitudes at sea level). Error due to scaling uncertainties is greatly minimized because of the close proximity between calibration sites and sample locations. For the ^{3}He age calculations, we use the altitudinal and latitudinal scaling factors of Lal (1991, Table 2) and thereby ignore production from muons.

We adopt a cosmogenic ^{10}Be production rate of 5.1 ± 0.3 atoms · g^{-1} · yr^{-1} (±2σ; in quartz, at high latitudes at sea level) (Stone, 2000; Gosse and Phillips, 2001). For the ^{10}Be age calculations, we use Stone's (2000) scaling factors, which modify the factors of Lal (1991; Table 2), to incorporate a muogenic component of 2.6% for ^{10}Be surface production at sea level. Lal (1991) estimated an uncertainty of 10% for his original scaling factors.

We make no correction for potential dipole-induced temporal variability of production rates at the Yellowstone field localities, and we use geographic latitude in scaling of production rates for the age calculations. This approach follows previous work suggesting that production rates at midlatitudes are relatively insensitive to changes in geomagnetic field strength (Cerling and Craig, 1994; Phillips et al., 1996; Licciardi et al., 1999), and assumes that the position of the dipole axis had sufficient time to average to the rotational pole over the exposure duration of the Yellowstone deposits (cf. Licciardi et al., 1999). In the case of the ^{3}He ages, uncertainties imparted by these effects are largely eliminated because the calibration surfaces are nearly identical in age to the calculated exposure durations and therefore integrate all relevant magnetic field effects on production.

UNCERTAINTIES

Although our sampling protocols were designed to minimize potential geological uncertainties derived from prior exposure, erosion, postdepositional movement, and burial, some of the observed age scatter in our data may be attributed to these phenomena. No erosion corrections were applied because many of the boulders selected for sampling exhibited glacial polish or striae. Concerns about fire-induced spalling of boulder surfaces are minimal because of the sparse vegetation on the moraines and as evidenced by preservation of striated surfaces. Uncertainty associated with thickness corrections is negligible, and the minimal shielding by surrounding topography largely eliminates the need for a correction. Annual snow cover is low at the field localities, as indicated by the available record of snow course data from nearby SNOTEL stations at similar elevations (average daily water-equivalent snow cover is <7 cm); therefore, no corrections were applied. The potential uncertainty associated with the lack of snow correction is probably 1%–2%.

Duplicate analyses were performed for four of the boulders sampled for ^{3}He measurements, and for eight of the boulders sampled for

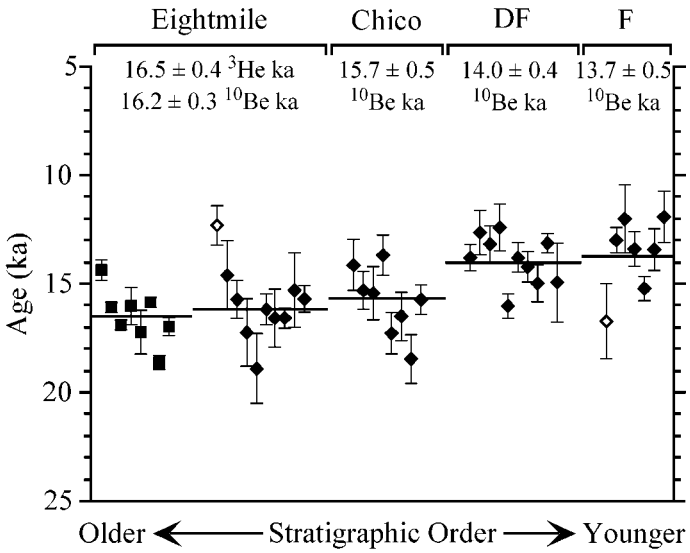

Figure 2. Ages of Yellowstone moraines, plotted in stratigraphic order from oldest (left side of graph) to youngest (right side). Squares are ^{3}He ages, and solid diamonds are ^{10}Be ages. Error bars on each age represent 1σ analytical uncertainty only, and do not include errors due to production rate, scaling, and other uncertainties. Horizontal lines and quoted ages indicate weighted means of each landform. Open diamonds indicate two outliers not included in weighted means. DF—Deckard Flats moraines; F—late-glacial flood deposits.

^{10}Be measurements. With one exception (sample 8B-4, Table 1[1]), the duplicate measurements overlap within 2σ error. For those boulders with duplicate analyses, the weighted mean of the two measurements is taken as the best representation of that boulder age.

We interpret the mean boulder exposure age, weighted according to estimated measurement precision (Bevington and Robinson, 1992, equation 4.17), as the best representation of landform age. The errors quoted for the weighted mean ages of each landform incorporate all propagated analytical uncertainties and are equivalent to the larger of either the internal analytical error or the weighted standard deviation of the weighted mean (Bevington and Robinson, 1992, equations 4.19 and 4.23). These uncertainties are unrealistically low in comparison to the true uncertainties, which must incorporate the estimated 2σ errors (~6%) in the production rates of cosmogenic ^{3}He and ^{10}Be, as well as qualitative estimates of additional error imparted by scaling uncertainties. The scatter within the age groupings that causes overlap among the range of ages for each moraine is equally likely to have its source in either analytical uncertainties or geological phenomena, and this ambiguity makes it difficult to constrain the duration of occupation for each moraine. Moreover, these difficulties suggest that the age differences between the landforms are approaching the resolution time of the cosmogenic ^{10}Be dating technique. Nevertheless, the coherency of the ^{10}Be data from each landform allows us to identify statistically significant age differences for events that occurred on millennial time scales (2–3 k.y.).

RESULTS

The 12 cosmogenic ^{3}He ages (derived from eight different boulders) on the Eightmile terminal moraines range from 18.6 ± 0.3 to 14.4 ± 0.5 ^{3}He ka; the weighted mean is 16.5 ± 0.4 ^{3}He ka (Table 1; see footnote 1) (Fig. 2). Of the 13 ^{10}Be measurements (derived from ten different boulders) on these moraines, only one boulder age (8-A) is considered an outlier (following Chauvenet's criterion; cf. Bevington and Robinson, 1992) and is not included in the weighted mean. The remaining boulder ages range from 18.9 ± 1.6 to 14.6 ± 1.6 ^{10}Be ka, the weighted mean being 16.2 ± 0.3 ^{10}Be ka (Table 2; see footnote 1) (Fig. 2). The weighted mean ^{10}Be age of the Eightmile moraines is ~2% lower than that obtained from the ^{3}He ages, and the age ranges from the two isotopes are nearly identical. These observations indicate that the ^{3}He and ^{10}Be ages are concordant within the combined error of production rates, scaling uncertainties, and measurement error. The production rates and scaling methodologies used in the age calculations from each isotope are thus likely to be reasonably accurate.

The ages obtained from nine ^{10}Be measurements (derived from eight different boulders) on the recessional Chico moraines range from 18.5 ± 1.1 to 13.7 ± 0.9 ^{10}Be ka; the weighted mean is 15.7 ± 0.5 ^{10}Be ka (Table 2; see footnote 1) (Fig. 2). Although the mean ^{10}Be age of the Chico moraines is slightly younger than that of the Eightmile terminal moraines, consistent with stratigraphic requirements, one-way ANOVA and post-hoc tests demonstrate that the difference in mean age of the two moraine complexes is not statistically significant. The ages therefore support field evidence suggesting that these two moraine-building events occurred within a short time period (Pierce, 1979).

Cosmogenic ^{10}Be ages obtained from 11 measurements on ten different boulders from the Deckard Flats moraine range from 16.0 ± 0.6 to 12.4 ± 1.1 ^{10}Be ka; the weighted mean is 14.0 ± 0.4 ^{10}Be ka (Table 2; see footnote 1) (Fig. 2). The ages obtained from ten ^{10}Be measurements (derived from seven different boulders, and excluding boulder F-1 as an anomalously old outlier) on the late-glacial flood deposit range from 15.2 ± 0.6 to 11.9 ± 1.2 ^{10}Be ka, the weighted mean being 13.7 ± 0.5 ^{10}Be ka. The age difference between the Deckard Flats moraine and the flood deposit is stratigraphically consistent but not statistically significant within uncertainties. The valley in the Deckard Flats region must have been largely ice-free during deposition of the flood bar; thus, these data imply a significant and rapid retreat of the Deckard Flats ice front after ~14 ^{10}Be ka.

COMPARISON TO EXISTING CHRONOLOGIES

On the basis of mass spectrometric U-series ages of travertines and carbonate veins thought to constrain glacier-driven changes in hydrological head in the northern Yellowstone area, Sturchio et al. (1994) proposed that the last Pinedale glacial maximum of the Yellowstone outlet glacier occurred between 30 and 22.5 ka, followed by a major recessional phase between 22.5 and 19.5 ka. They constrained the duration of the subsequent Deckard Flats glacial event from two U-series ages on an aragonite vein on a travertine bench on Deckard Flats (Fig. 1C) as occurring between 20.2 and 15.5 ka. Subsequent cessation of vein deposition signified final retreat of the Deckard Flats glacier from the Gardiner area, and postglacial travertine deposits indicate that glaciers had probably receded well upvalley from Deckard Flats by no later than 14–13 ka (Sturchio et al., 1994).

The presence of subaerial travertines dated by Sturchio et al. (1994) at 22.5–19.5 ka indicates that there was no ice covering the Deckard Flats bench during this time interval. Our cosmogenic ages on the Eightmile and Chico moraines, however, conflict with the interpretation by Sturchio et al. (1994) that continuous accumulation of vein aragonite between 20.2 and 15.5 ka implies restricted ice at Deckard Flats during this time. We suggest that either vein aragonite may have formed in the subsurface beneath the ice or there may be an unrecognized hiatus between the 20.2 ka and 15.5 ka bracketing U-series ages on the vein aragonite, during which the Yellowstone outlet glacier advanced to the Eightmile and Chico moraines. If the latter is accurate, then the combined data sets suggest that the Yellowstone outlet glacier was in a recessional position from 22.5 to 19.5 ka and advanced to its maximum extent at ~16.5 ka. Our cosmogenic age for

[1]GSA Data Repository item 2001127, Table 1, Helium data for Eightmile terminal moraines, and Table 2, Beryllium data for Yellowstone moraines, is available on request from Documents Secretary, GSA, P.O. Box 9140, Boulder, CO 80301, editing@geosociety.org, or at www.geosociety.org/pubs/ft2001.htm.

the Chico moraine (15.7 ^{10}Be ka) and the younger U-series age of the vein aragonite from Deckard Flats (15.5 ka) may suggest rapid ice-margin retreat at ~15.5 ka. Finally, we suggest that occupation of the Deckard Flats ice limit at ~14 ^{10}Be ka may represent an event that was not recorded by travertine or vein deposition, or simply not represented in the samples collected by Sturchio et al. (1994).

Our cosmogenic evidence for a fully expanded northern Yellowstone outlet glacier at ~16.5 ^{10}Be ka is in apparent conflict with radiocarbon evidence for near-complete deglaciation of the Yellowstone plateau by ~14.5–14 ^{14}C ka (~17.4–16.8 cal ka). A suite of conventional radiocarbon ages from bulk sediment and other materials near Yellowstone Lake indicates a minimum age of ~14 ^{14}C ka for deglaciation of the Yellowstone plateau (Pierce, 1979; Richmond, 1986). A basal radiocarbon age on sediment from a core at Cygnet Lake, on the central plateau, indicates that this region was ice-free even earlier, by ~14.5 ^{14}C ka (Whitlock, 1993; Millspaugh et al., 2000). However, Whitlock (1993) suggested that the Cygnet Lake radiocarbon age should be considered a maximum age, because of low organic content and the possibility that the samples were contaminated by ^{14}C-free organic material, and we suspect the same is true for other old radiocarbon ages measured on bulk sediment in the central plateau region (Pierce, 1979).

Formation of the Deckard Flats moraines at ~14 ^{10}Be ka is consistent with deglaciation of the Yellowstone plateau by 13.5 cal ka, as suggested by the presence of Glacier Peak tephra in Cygnet Lake sediments (Whitlock, 1993). Pierce (1979) interpreted the Deckard Flats moraines as being deposited when the Yellowstone ice cap deglaciated and the source region of the Yellowstone outlet glacier changed to ice from the adjacent Beartooth uplift and Gallatin Range (Fig. 1A).

CONCLUSIONS

Cosmogenic ages from the maximum Pinedale terminal moraines indicate a fully extended northern Yellowstone outlet glacier at 16.5 ± 0.4 ^{3}He ka and 16.2 ± 0.3 ^{10}Be ka. This age is significantly younger than previously thought for the late Pinedale maximum extent of the outlet glacier (Pierce, 1979; Sturchio et al., 1994), and for the late Pinedale maximum elsewhere in much of the Rocky Mountains (Porter et al., 1983; Gosse et al., 1995). Our new ages are similar, however, to the age of the maximum extent of the Puget Lobe of the Cordilleran ice sheet (~16.9 cal ka) (Porter and Swanson, 1998).

Our ages on the Deckard Flats moraines are consistent with the hypothesis that ice from the Beartooth uplift and the Gallatin Range was the primary source of Deckard Flats ice, with little or no contribution from the plateau ice masses to the south (Pierce, 1979). Because these source regions have a higher average elevation and a greater area above the inferred Pleistocene equilibrium-line altitude than the Yellowstone ice cap, ice would have persisted there longer than the ice cap on the central plateau during deglaciation (Pierce, 1979), and their contribution to the outlet glacier relative to the plateau ice cap increased over time as deglaciation progressed. Our new cosmogenic data therefore suggest that disintegration of the plateau ice cap was well under way by 14 ^{10}Be ka.

ACKNOWLEDGMENTS

We thank J.O. Stone, D.E. Granger, M. Bourgeois, J.C. Gosse, S. Vogt, and G.P. Landis for many helpful suggestions and for providing unpublished data and manuscripts; S.H. Bloomer, A. Ungerer, and K.K. Falkner for use of laboratory facilities; J.M. Curtice and R.P. Ackert Jr. for assistance with helium measurements; R.L. Nielsen and E. Kohut for assistance with microprobe analyses; J. Clark for field assistance; J.S. Heaton for help with statistics; A.M. Heimsath and D. Lal for comments; and the many private landowners in the field areas for kindly permitting access to sites. We especially thank T. Miller and other personnel at PRIME Lab for their perseverance and patience with this project. Supported by the National Science Foundation, the Geological Society of America, Sigma Xi, and the Oregon Research Council. This is Woods Hole Oceanographic Institution contribution 10490.

REFERENCES CITED

Bevington, P.R., and Robinson, D.K., 1992, Data reduction and error analysis for the physical sciences: Boston, WCB/McGraw-Hill, 328 p.

Brown, E.T., Brook, E.J., Raisbeck, G.M., Yiou, F., and Kurz, M.D., 1992, Effective attenuation lengths of cosmic rays producing ^{10}Be and ^{26}Al in quartz: Implications for exposure age dating: Geophysical Research Letters, v. 19, p. 369–372.

Cerling, T.E., and Craig, H., 1994, Cosmogenic ^{3}He production rates from 39° to 46°N latitude, western USA and France: Geochimica et Cosmochimica Acta, v. 58, p. 249–255.

Gosse, J.C., and Phillips, F.M., 2001, Terrestrial in situ cosmogenic nuclides: Theory and application: Quaternary Science Reviews, v. 20, p. 1475–1560.

Gosse, J.C., Klein, J., Evenson, E.B., Lawn, B., and Middleton, R., 1995, Beryllium-10 dating of the duration and retreat of the last Pinedale glacial sequence: Science, v. 268, p. 1329–1333.

Kohl, C.P., and Nishiizumi, K., 1992, Chemical isolation of quartz for measurement of in-situ–produced cosmogenic nuclides: Geochimica et Cosmochimica Acta, v. 56, p. 3583–3587.

Kurz, M.D., 1986, In situ production of terrestrial cosmogenic helium and some applications to geochronology: Geochimica et Cosmochimica Acta, v. 50, p. 2855–2862.

Kurz, M.D., Colodner, D., Trull, T.W., Moore, R.B., and O'Brien, K., 1990, Cosmic ray exposure dating with in situ produced cosmogenic ^{3}He: Results from young Hawaiian lava flows: Earth and Planetary Science Letters, v. 97, p. 177–189.

Kurz, M.D., Kenna, T.C., Lassiter, J.C., and DePaolo, D.J., 1996, Helium isotopic evolution of Mauna Kea volcano: First results from the 1 km drill core: Journal of Geophysical Research, v. 101, p. 11 781–11 791.

Lal, D., 1991, Cosmic ray labeling of erosion surfaces: In-situ nuclide production rates and erosion models: Earth and Planetary Science Letters, v. 104, p. 424–439.

Licciardi, J.M., 2000, Alpine glacier and pluvial lake records of late Pleistocene climate variability in the western United States [Ph.D. thesis]: Corvallis, Oregon State University, 155 p.

Licciardi, J.M., Kurz, M.D., Clark, P.U., and Brook, E.J., 1999, Calibration of cosmogenic ^{3}He production rates from Holocene lava flows in Oregon, USA, and effects of the Earth's magnetic field: Earth and Planetary Science Letters, v. 172, p. 261–271.

Millspaugh, S.H., Whitlock, C., and Bartlein, P.J., 2000, Variations in fire frequency and climate over the past 17 000 yr in central Yellowstone National Park: Geology, v. 28, p. 211–214.

Phillips, F.M., Zreda, M.G., Flinsch, M.R., Elmore, D., and Sharma, P., 1996, A reevaluation of cosmogenic ^{36}Cl production rates in terrestrial rocks: Geophysical Research Letters, v. 23, p. 949–952.

Pierce, K.L., 1979, History and dynamics of glaciation in the northern Yellowstone National Park area: U.S. Geological Survey Professional Paper 729-F, 90 p.

Pierce, K.L., Obradovich, J.D., and Friedman, I., 1976, Obsidian hydration dating and correlation of Bull Lake and Pinedale glaciations near West Yellowstone, Montana: Geological Society of America Bulletin, v. 87, p. 703–710.

Porter, S.C., and Swanson, T.W., 1998, Radiocarbon age constraints on rates of advance and retreat of the Puget Lobe of the Cordilleran ice sheet during the last glaciation: Quaternary Research, v. 50, p. 205–213.

Porter, S.C., Pierce, K.L., and Hamilton, T.D., 1983, Late Wisconsin mountain glaciation in the western United States, *in* Porter, S.C., ed., Late-Quaternary environments of the United States. Volume 1. The late Pleistocene: Minneapolis, University of Minnesota Press, p. 71–111.

Richmond, G.M., 1986, Stratigraphy and chronology of glaciations in Yellowstone National Park, *in* Sibrava, V., et al., eds., Quaternary glaciations in the Northern Hemisphere: Quaternary Science Reviews, v. 5, p. 83–98.

Sharma, P., Bourgeois, M., Elmore, D., Granger, D., Lipschutz, M.E., Ma, X., Miller, T., Mueller, K., Rickey, F., Simms, P., and Vogt, S., 2000, PRIME Lab AMS performance, upgrades, and research applications: Nuclear Instruments and Methods in Physics Research, v. B172, p. 112–123.

Stone, J.O., 2000, Air pressure and cosmogenic isotope production: Journal of Geophysical Research, v. 105, p. 23 753–23 759.

Sturchio, N.C., Pierce, K.L., Murrell, M.T., and Sorey, M.L., 1994, Uranium-series ages of travertines and timing of the last glaciation in the northern Yellowstone area, Wyoming-Montana: Quaternary Research, v. 41, p. 265–277.

Whitlock, C., 1993, Postglacial vegetation and climate of Grand Teton and southern Yellowstone National Parks: Ecological Monographs, v. 63, p. 173–198.

Manuscript received April 23, 2001
Revised manuscript received July 20, 2001
Manuscript accepted August 7, 2001

Printed in USA

GSA Data Repository Item 2001127, Table DR1, Helium data for Eightmile terminal moraines, and Table DR2, Beryllium data for Yellowstone moraines.

Table DR1. Helium data for Eightmile terminal moraines. Duplicate ^{3}He measurements on splits of olivine from the same boulder, prepared separately for analysis, are labeled 8B-1A and 8B-1B, etc. Olivine compositions (expressed as forsterite content) are mean values and sample standard deviations derived from individual electron microprobe measurements on at least five phenocrysts from each sample location. The narrow range of compositions exhibited by the analyzed olivine phenocrysts (from Fo_{77} to Fo_{83}) suggests that compositional differences are an unlikely source of scatter in the ^{3}He ages (cf. Lal, 1991). Helium measurement uncertainties are based on 0.5% uncertainty on the ^{4}He peak and an error of 2×10^{-12} cm^3 STP (about 3%) on the blank. We do not correct for implantation of radiogenic ^{4}He (cf. Brook et al., 1995; Kurz et al, 1996; Dunai and Wijbrans, 2000) in our calculations, and we assume the potential effects to be within the range of measurement uncertainty. ^{3}He/^{4}He ratios are reported relative to the atmospheric value (R/R_a, where $R_a = 1.384 \times 10^{-6}$). For all samples, crushing and melting were performed on the same mineral separate. Crushed ^{4}He contents were relatively low (7.4×10^{-11} to 5.4×10^{-10} cm^3 STP), leading to significant blank corrections for some of the inherited ^{3}He/^{4}He ratios (blank values ranged from 4.7 to 6.6×10^{-11} cm^3 STP). The large blank corrections for the inherited ^{4}He, however, contribute minimal error to the calculated ^{3}He ages because of the comparatively large amounts of cosmogenic ^{3}He and the high reproducibility of the blanks. Weighted means of duplicate measurements of inherited ^{3}He/^{4}He ratios were used for age calculations. "#" indicates ^3He_c concentrations normalized to the surface. Thickness corrections assume an attenuation coefficient of 170 g·cm^{-2} (Kurz, 1986) and a rock density of 3.1 g·cm^{-3}. Scaling factors are the ratio of production at sample location to production at high latitudes at sea level, following Lal (1991, table 2). All quoted uncertainties are 1σ, and incorporate analytical error only. The magnitude of additional uncertainties is discussed in the text.

Table DR1. Helium data for Eightmile terminal moraines.

Sample	Olivine (g)	Oliv. Comp.	Thickness (cm)	Alt. (km)	Lat. (deg. N)	Lon. (deg. W)	$^3He/^4He$ (R/R_a, crush)	$^3He/^4He$ (R/R_a, melt)	^4He (10^{-9} cm^3 g^{-1})	^3He_c (10^5 at g^{-1})	$^3He_c^{\#}$ (10^5 at g^{-1})	Scaling factor	Age (^{3}He ka)
8B-1A	0.287	$Fo_{77\pm5}$	2.00	1.529	45.436	110.690	17.79 ± 2.66	97.97 ± 0.58	2.10 ± 0.01	60.14 ± 2.59	61.24 ± 2.63	3.56	14.5 ± 0.6
8B-1B	0.206	$Fo_{77\pm5}$	2.00	1.529	45.436	110.690	24.22 ± 2.80	92.57 ± 0.64	2.23 ± 0.01	59.40 ± 2.76	60.49 ± 2.81	3.56	14.3 ± 0.7
8B-2	0.285	$Fo_{82\pm1}$	2.50	1.529	45.436	110.690	18.66 ± 0.37	96.31 ± 0.60	2.31 ± 0.01	66.64 ± 0.78	68.18 ± 0.80	3.56	16.2 ± 0.2
8B-3	0.291	$Fo_{81\pm1}$	2.50	1.529	45.436	110.690	17.89 ± 0.58	133.73 ± 0.79	1.62 ± 0.01	69.81 ± 0.80	71.42 ± 0.82	3.56	16.9 ± 0.2
8B-4A	0.229	$Fo_{82\pm2}$	2.25	1.538	45.436	110.693	21.19 ± 2.36	110.67 ± 0.81	2.10 ± 0.01	70.09 ± 0.90	71.53 ± 0.92	3.58	16.8 ± 0.2
8B-4B	0.327	$Fo_{82\pm2}$	2.25	1.538	45.436	110.693	21.17 ± 0.36	77.04 ± 0.30	3.03 ± 0.02	63.10 ± 0.72	64.40 ± 0.73	3.58	15.2 ± 0.2
8B-5	0.134	$Fo_{83\pm2}$	3.00	1.541	45.434	110.692	18.54 ± 3.06	73.51 ± 0.51	3.49 ± 0.02	71.49 ± 4.09	73.46 ± 4.20	3.59	17.3 ± 1.0
8B-6	0.147	$Fo_{83\pm1}$	2.50	1.529	45.435	110.688	10.04 ± 0.28	51.65 ± 0.44	4.24 ± 0.03	65.61 ± 0.96	67.12 ± 0.98	3.56	15.9 ± 0.2
8B-7A	0.263	$Fo_{79\pm3}$	3.00	1.530	45.436	110.686	4.56 ± 0.35	185.49 ± 1.14	1.15 ± 0.01	77.56 ± 0.83	79.70 ± 0.85	3.56	18.9 ± 0.2
8B-7B	0.224	$Fo_{79\pm3}$	3.00	1.530	45.436	110.686	4.08 ± 0.40	119.03 ± 0.90	1.76 ± 0.01	75.26 ± 0.83	77.33 ± 0.85	3.56	18.3 ± 0.2
8B-8A	0.275	$Fo_{81\pm1}$	1.50	1.530	45.436	110.687	16.70 ± 1.06	135.28 ± 1.01	1.64 ± 0.01	72.50 ± 0.94	73.49 ± 0.95	3.56	17.4 ± 0.2
8B-8B	0.287	$Fo_{81\pm1}$	1.50	1.530	45.436	110.687	16.67 ± 0.95	120.69 ± 0.73	1.79 ± 0.00	69.27 ± 0.85	70.22 ± 0.86	3.56	16.6 ± 0.2

Table DR2. Beryllium data for Yellowstone moraines. Duplicate ^{10}Be measurements on splits of quartz from the same boulder, prepared separately for analysis, are labeled 8-J1 and 8-J2, CH-6A and CH-6B, etc. The ^{10}Be data are normalized with respect to a standard reference material (SRM 4325) obtained from the National Institute of Standards and Technology, and a correction was incorporated for the discrepancy of 14% reported by Middleton et al. (1993) for SRM 4325 (cf. Sharma et al., 2000). The largest potential contributor to analytical uncertainty of the ^{10}Be measurements is isobaric interference of ^{10}B with ^{10}Be. We rejected all measurements with high boron interference, thereby minimizing uncertainties imparted by this effect. The precision of the ^{10}Be measurements is dependent in part on the degree of isobaric ^{10}B interference and on the counting time and ^{10}Be activity level. Because these parameters varied widely among the samples, so does the associated measurement precision. Analyses of 13 chemical blanks yielded ^{10}Be/^{9}Be ratios that range from 0.5 to 7.8×10^{-15} and have a mean value of 3.2×10^{-15}, which is comparable to the ^{10}Be/^{9}Be background level of the accelerator mass spectrometer at the PRIME Lab facility (Sharma et al., 2000). These results indicate that laboratory contamination with meteoric ^{10}Be is not a problem for our samples. "#" indicates cosmogenic ^{10}Be concentrations normalized to the surface. Thickness corrections assume an attenuation coefficient of 145 g·cm^{-2} (Brown et al., 1992) and a rock density of 2.8 g·cm^{-3}. Scaling factors are the ratio of production at sample locations to production at high latitudes at sea level, following Stone (2000). All quoted uncertainties are 1σ, and incorporate analytical error only. The magnitude of additional uncertainties is discussed in the text.

Table DR2. Beryllium data for Yellowstone moraines.

Sample	Quartz (g)	Thickness (cm)	Altitude (km)	Latitude (deg. N)	Longitude (deg. W)	^{10}Be (10^5 at g^{-1})	^{10}Be# (10^5 at g^{-1})	Scaling factor	Age (^{10}Be ka)
Eightmile Terminal Moraines									
8-A2	40.011	1.00	1.548	45.432	110.700	2.21 ± 0.17	2.23 ± 0.17	3.57	12.3 ± 0.9
8-B2	21.874	2.50	1.550	45.429	110.707	2.59 ± 0.29	2.66 ± 0.29	3.57	14.6 ± 1.6
8-D1	29.049	0.75	1.545	45.429	110.705	2.83 ± 0.16	2.85 ± 0.16	3.56	15.7 ± 0.9
8-F2	18.841	1.50	1.544	45.437	110.695	3.08 ± 0.28	3.13 ± 0.29	3.56	17.3 ± 1.6
8-G2	21.504	1.00	1.529	45.436	110.691	3.34 ± 0.28	3.38 ± 0.28	3.52	18.9 ± 1.6
8-I1	30.089	1.75	1.529	45.435	110.690	2.82 ± 0.14	2.86 ± 0.14	3.52	16.0 ± 0.8
8-I2	21.839	1.75	1.529	45.435	110.690	3.00 ± 0.26	3.05 ± 0.27	3.52	17.1 ± 1.5
8-J1	28.108	2.00	1.554	45.365	110.690	2.81 ± 0.38	2.86 ± 0.39	3.58	15.7 ± 2.2
8-J2	20.938	2.00	1.554	45.365	110.690	3.10 ± 0.33	3.16 ± 0.34	3.58	17.3 ± 1.9
8-K1	30.238	2.75	1.536	45.429	110.688	2.91 ± 0.10	2.99 ± 0.10	3.54	16.6 ± 0.5
8-L1	21.229	3.00	1.554	45.365	110.690	2.22 ± 0.23	2.29 ± 0.24	3.58	12.5 ± 1.3
8-L2	20.713	3.00	1.554	45.365	110.690	2.89 ± 0.14	2.98 ± 0.14	3.58	16.4 ± 0.8
8-M2	19.915	2.50	1.561	45.363	110.691	2.80 ± 0.11	2.87 ± 0.11	3.60	15.7 ± 0.6
Chico Moraines									
CH-1A	30.003	2.50	1.628	45.339	110.698	2.64 ± 0.22	2.70 ± 0.23	3.78	14.1 ± 1.2
CH-2A	32.923	1.75	1.634	45.337	110.697	2.90 ± 0.18	2.95 ± 0.18	3.80	15.3 ± 0.9
CH-3B	25.857	1.75	1.652	45.334	110.695	2.98 ± 0.26	3.03 ± 0.26	3.85	15.5 ± 1.3
CH-6A	37.241	1.75	1.615	45.335	110.705	2.64 ± 0.22	2.69 ± 0.22	3.75	14.1 ± 1.2
CH-6B	30.022	1.75	1.615	45.335	110.705	2.48 ± 0.27	2.52 ± 0.27	3.75	13.2 ± 1.4
CH-8A	24.371	0.75	1.615	45.336	110.704	3.27 ± 0.19	3.29 ± 0.19	3.75	17.3 ± 1.0
CH-9B	21.511	1.75	1.618	45.338	110.703	3.10 ± 0.21	3.15 ± 0.22	3.75	16.5 ± 1.1
CH-10B	28.763	1.25	1.612	45.340	110.703	3.47 ± 0.20	3.52 ± 0.21	3.74	18.5 ± 1.1
CH-11B	25.669	0.75	1.615	45.342	110.703	2.97 ± 0.14	2.99 ± 0.14	3.75	15.7 ± 0.7
Deckard Flats Moraines									
DF-1A	40.079	0.75	1.811	45.039	110.685	2.99 ± 0.13	3.01 ± 0.14	4.30	13.8 ± 0.6
DF-2B	32.035	1.75	1.811	45.039	110.685	2.71 ± 0.25	2.75 ± 0.25	4.30	12.6 ± 1.1
DF-3B	18.359	1.75	1.811	45.039	110.685	2.83 ± 0.19	2.88 ± 0.19	4.30	13.2 ± 0.9
DF-4A	25.067	1.75	1.811	45.039	110.685	2.67 ± 0.23	2.71 ± 0.23	4.30	12.4 ± 1.1
DF-5B	24.667	1.50	1.811	45.039	110.685	3.45 ± 0.14	3.50 ± 0.14	4.30	16.0 ± 0.7
DF-6A	25.124	1.75	1.811	45.039	110.685	2.88 ± 0.15	2.93 ± 0.15	4.30	13.4 ± 0.7
DF-6B	24.725	1.75	1.811	45.039	110.685	3.19 ± 0.24	3.25 ± 0.25	4.30	14.9 ± 1.1
DF-7A	40.038	1.50	1.811	45.039	110.685	3.07 ± 0.16	3.11 ± 0.16	4.30	14.2 ± 0.7
DF-8A	24.807	1.25	1.807	45.038	110.685	3.23 ± 0.19	3.26 ± 0.19	4.29	15.0 ± 0.9
DF-9B	30.054	1.75	1.804	45.038	110.684	2.81 ± 0.11	2.86 ± 0.11	4.28	13.1 ± 0.5
DF-10A	24.299	0.75	1.801	45.038	110.683	3.22 ± 0.39	3.24 ± 0.39	4.27	14.9 ± 1.8
Flood Deposit									
F-1A	22.024	0.50	1.583	45.056	110.764	3.07 ± 0.33	3.09 ± 0.34	3.64	16.7 ± 1.8
F-3A	25.013	1.50	1.583	45.056	110.764	2.25 ± 0.14	2.28 ± 0.15	3.64	12.3 ± 0.8
F-3B	24.146	1.50	1.583	45.056	110.764	2.46 ± 0.13	2.50 ± 0.13	3.64	13.5 ± 0.7
F-4A	25.015	0.50	1.584	45.056	110.764	2.21 ± 0.29	2.22 ± 0.29	3.64	12.0 ± 1.6
F-6A	25.012	1.50	1.584	45.056	110.764	2.30 ± 0.13	2.33 ± 0.13	3.64	12.6 ± 0.7
F-6B	24.171	1.50	1.584	45.056	110.764	2.57 ± 0.14	2.61 ± 0.14	3.64	14.1 ± 0.7
F-9A	26.856	2.00	1.585	45.057	110.764	2.72 ± 0.14	2.78 ± 0.14	3.65	15.0 ± 0.8
F-9B	25.203	2.00	1.585	45.057	110.764	2.79 ± 0.14	2.84 ± 0.15	3.65	15.3 ± 0.8
F-10B	40.138	1.50	1.585	45.057	110.764	2.45 ± 0.17	2.49 ± 0.18	3.65	13.4 ± 1.0
F-11A	25.020	1.50	1.584	45.056	110.764	2.19 ± 0.23	2.20 ± 0.23	3.64	11.9 ± 1.2

REFERENCES CITED (GSA Data Repository Item 2001XXX)

Brook, E.J., Kurz, M.D., Ackert, R.P., Raisbeck, G.M., and Yiou, F., 1995, Cosmogenic nuclide exposure ages and glacial history of late Quaternary Ross Sea drift in McMurdo Sound, Antarctica: Earth and Planetary Science Letters, v. 131, p. 41-56.

Brown, E.T., Brook, E.J., Raisbeck, G.M., Yiou, F., and Kurz, M.D., 1992, Effective attenuation lengths of cosmic rays producing ^{10}Be and ^{26}Al in quartz: Implications for exposure age dating: Geophysical Research Letters, v. 19, p. 369-372.

Dunai, T.J., and Wijbrans, J.R., 2000, Long-term cosmogenic ^{3}He production rates (152 ka-1.35 Ma) from ^{40}Ar/^{39}Ar dated basalt flows at 29°N latitude: Earth and Planetary Science Letters, v. 176, p. 147-156.

Kurz, M.D., 1986, In situ production of terrestrial cosmogenic helium and some applications to geochronology: Geochimica et Cosmochimica Acta, v. 50, p. 2855-2862.

Kurz, M.D., Kenna, T.C., Lassiter, J.C., and DePaolo, D.J., 1996, Helium isotopic evolution of Mauna Kea Volcano: First results from the 1 km drill core: Journal of Geophysical Research, v. 101, p. 11,781-11,791.

Lal, D., 1991, Cosmic ray labeling of erosion surfaces: In-situ nuclide production rates and erosion models: Earth and Planetary Science Letters, v. 104, p. 424-439.

Middleton, R., Brown, L., Dezfouly-Arjomandy, B., and Klein, J., 1993, On ^{10}Be standards and the half life of ^{10}Be: Nuclear Instruments and Methods in Physics Research, v. B82, p. 399-403.

Sharma, P., Bourgeois, M., Elmore, D., Granger, D., Lipschutz, M.E., Ma, X., Miller, T., Mueller, K., Rickey, F., Simms, P., and Vogt, S., 2000, PRIME Lab AMS performance, upgrades, and research applications: Nuclear Instruments and Methods in Physics Research, v. B172, p. 112-123.

Stone, J.O., 2000, Air pressure and cosmogenic isotope production: Journal of Geophysical Research, v. 105, p. 23 753-23 759.